Open access • Proceedings Article • DOI:10.2514/6.2019-0822

Performance enhancement of gust load alleviation systemsfor flexible aircraft using H_infinity optimal control with preview — Source link

Ahmed Khalil Ali Khalil, Nicolas Fezans

Institutions: German Aerospace Center

Published on: 06 Jan 2019

Topics: Range (aeronautics), Feed forward, Control theory, Optimal control and Control system

AIAA SciTech Forum
7-11 January 2019, San Diego, California
AIAA Scitech 2019 Forum

10.2514/6.2019-0822

Performance Enhancement of Gust Load Alleviation Systems for Flexible Aircraft using H_∞ Optimal Control with Preview

Ahmed Khalil* and Nicolas Fezans†
DLR (German Aerospace Center), Lilienthalplatz 7, 38108 Braunschweig, Germany

Most of the gust load alleviation systems (GLAS) of currently-operational aircraft are of feedback-only control architecture based on inertial measurements. In few other aircraft, aerodynamic measurements from air data sensors are additionally included, or presently considered for inclusion, as they usually result in improving the performance of the GLAS. In both sensor types, the control system has very little time to react; and therefore, the performance of the GLAS would be further enhanced if the turbulence or gust could be measured at some distance ahead of the aircraft. Doppler LIDAR (LIght Detection And Ranging) sensors could enable such preview of the turbulence or gust, at a short range (typically between 30 and 200 meters) ahead of the aircraft. In this paper, the availability of a vertical wind profile ahead of the aircraft is assumed, and the paper focuses on the design of a load alleviation controller that exploits this information. The proposed methodology of designing this controller is based on the application of the H_∞ optimal control techniques to a discrete-time preview control problem. Minimizing the H_∞ norm of the transfer function from wind input to loads output, directly leads to the design of an effective load alleviation function. The preview-control formulation enables the design algorithm to synthesize a combined preview-capable feedforward and feedback load alleviation function. For a practical reason, the developed methodology is applied in the course of this paper to a flexible sailplane model (DLR's Discus-2c), although it is intended to be applied to larger airplanes (e.g. transport airplanes and business jets).

I. Nomenclature

Some of the standard symbols used in flight mechanics are also used in control theory. In order to avoid any confusion, a **bold** font is used when the symbol is for control theory, while a regular font is used when the symbol is for flight mechanics. Distinction between the two will also be made throughout the paper if ambiguity might arise. The symbols for flight mechanics are according to the ISO Standard 1151 (see [1, 2]).

Flight Mechanics and Structural Dynamics:

CG	=	center of gravity of the aircraft
g	=	Earth's gravity
$I_{..}$	=	moments and products of inertia of the aircraft with respect to the body axis system (. = x, y or z)
L, M, N	=	components of the resultant moment about the CG in the body axis system
m	=	aircraft mass
p, q, r	=	components of the aircraft angular velocity vector in the body axis system
u, v, w	=	components of the velocity vector of the aircraft relative to the air in the body axis system
u_K, v_K, w_K	=	components of the velocity vector of the aircraft relative to the Earth in the body axis system
u_W, v_W, w_W	=	components of the velocity vector of the wind relative to the Earth in the body axis system
V_∞	=	true airspeed
X, Y, Z	=	components of the resultant force vector in the body axis system
xyz	=	body axis system (fixed in the aircraft, with the origin, the CG)
x, y, z	=	inertial displacements
α, α_K	=	angle of attack and kinematic angle of attack, respectively

*PhD Candidate, Institute of Flight Systems, Lilienthalplatz 7, 38108 Braunschweig, Germany, ahmed.khalil@dlr.de.
†Scientific Advisor, Institute of Flight Systems, Lilienthalplatz 7, 38108 Braunschweig, Germany, AIAA Corporate Member.

Φ, Θ, Ψ = 3-2-1 Euler angels (bank, inclination and azimuth angles, respectively)
d_E = total elastic deformation
m_i , Q_i = generalized mass and force, respectively
ζ_i, ω_i = modal damping and natural frequency, respectively
η_i = generalized coordinate associated with the i^{th} vibration mode
ϕ_i = vibration mode shape (eigenfunction)

Control:

$\boldsymbol{d}$ = disturbance input
$\boldsymbol{d_p}$ = previewed disturbance input available for the control action
$H_\infty, \|.\|_\infty$ = infinity norm
$\boldsymbol{h}$ = preview time (continuous-time) or preview length (discrete-time)
T_{zw} = closed-loop transfer matrix from the exogenous input to the regulated output
$\boldsymbol{u}$ = control input
$\boldsymbol{w}$ = exogenous input
$\boldsymbol{x}$ = system states
$\boldsymbol{y}$ = measured output
$\boldsymbol{z}$ = regulated output
γ = H_∞ performance value
ξ = augmented state vector

II. Introduction

Turbulence and gusts are causing variations of the aerodynamic forces and moments that are applied to the aircraft structure. In addition to causing dynamic structural loads that the structure should be designed to support, these variations of forces and moments also cause passenger discomfort and anxiety. Active load alleviation of turbulence and gusts is not a new topic: the investigations made on the Lockheed C-5A to solve its fatigue issues leading to the development of the Active Lift Distribution Control System (ALDCS) dates back forty years [3]. Over the last decades, many GLAS had been implemented on numerous airplanes, such as: Lockheed C-5A, Lockheed L-1011-500, Boeing B-1, Airbus A320, Airbus A330/A340, Airbus A380 and Airbus A350. The GLAS of these airplanes were mainly of feedback-only control architecture based on inertial measurements (i.e., accelerometers), see [4].

In some other airplanes (e.g., Northrop Grumman B-2 and Boeing 787), aerodynamic measurements (i.e., static air data sensors) were additionally included to estimate the gust component of the airplane angle of attack [4]. The feedforward control problem then becomes a question of applying the right control action at the right time, whereas the angle of attack measurements are taken ahead of the wing (e.g. at the aircraft nose) in an attempt to compensate for the time delays in the control loop. DLR's research activities in this direction led to the Open-Loop Gust Alleviation (OLGA) [5–7] and the Load Alleviation and Ride Smoothing (LARS) [8–10] systems. The limiting factors are in this case the finite number of independent actuators (e.g., direct-lift control (DLC) flaps and ailerons) and their bandwidth. For instance, the DLC flaps of the DLR former test aircraft ATTAS (modified VFW-614) were having an authority on the vertical load factor of around ±0.3 g, which is indeed less than what is needed in case of large amplitude gusts.

The numerous successes of active control technologies for gust alleviation logically ended up reaching the maximum technology readiness level (TRL) of 9 for some of these systems. Consequently, the orientation of DLR's research activities on gust alleviation moved from the design of gust alleviation systems that are based on classical sensors (such as in the OLGA or the LARS systems) to the investigation of the potential performance enhancement that would result from the use of more advanced/futuristic sensors. The previous work that had been performed in these directions, especially during the AWIATOR project, led in particular to the GCS [11] and the GLA [12–14] systems, and to also consider the use of Doppler LIDAR sensors for determination of wind ahead of the aircraft for load alleviation purposes [11–20].

By pitching the aircraft up or down, angle of attack variations can be commanded, leading to effective variations in terms of loads much larger than with control surfaces on the wing. Optimally, combining wing control surface deflections and pitching actions therefore permits to improve the load alleviation performance, compared to what can be achieved with wing control surface deflections only. It is also crucial to understand that this increase in achievable

load performance depends on the lead-time for the disturbance (here turbulence or gusts), i.e. how long in advance the turbulence or gusts are determined. When additionally considering the effects related to the aircraft flexibility (change of shape of the aerodynamic surfaces plus inertial accelerations) and to the unsteady aerodynamics behavior, the design of an optimal load alleviation controller is even less straightforward than in the rigid-aircraft steady aerodynamics case. The methodology proposed in this paper provides a good compromise between performance and tuning flexibility.

As in the previously mentioned work, the feedforward load alleviation function designed with the methodology presented afterwards is based on the observation that with more anticipation of the near future loads, a higher load alleviation performance can be achieved. This is realized by gathering information on the wind field ahead of the aircraft, which in the current concept is based on a Doppler LIDAR sensor and a rather extensive processing of the obtained measurements. The current work benefits from what had been achieved in the previously mentioned work and projects, but focuses mainly on improving the controller design step. To do so, the problem of previewing the turbulence or gusts is formulated in a mathematical way that could be used by the already available control synthesis techniques.

III. Considered Application and Models Used

In this section, the flexible aircraft will be introduced, then a general aeroelastic model of it will be presented, and finally the model used for this work will be described.

A. The DLR Discus-2c Sailplane

Although this work is primarily intended to be applied on large transport aircraft (Part 25 of the FAA airworthiness standards or the EASA certification specifications), an aeroelastic model of a sailplane is used in this work for reasons related to the model availability and intellectual property. The relative simplicity of this model, compared to models extracted from coupled CFD/CSM tools, makes it also easier to test new ideas and methodologies on this model than with most CFD/CSM-derived models. The aircraft used for the simulation is the high-performance single-seat DLR's Discus-2c sailplane shown in Fig. 1, and has the general mass and geometry characteristics given in Table. 1.

A flight test measurement system is installed to the aircraft and consists of (among others) a 5-hole probe nose boom, GPS, INS, 46 strain gauge sensors and 15 three-axis accelerometers at different aircraft locations indicated in Fig. 2. In this work, only the symmetric motion and loads are considered. The considered locations and loads for the control synthesis will be given later with more details in the results section.

Fig. 1 DLR's Discus-2c Sailplane in Flight

B. The Discus-2c Aeroelastic Simulation Model

A nonlinear flexible model of this aircraft has been developed based on ground tests, flight test data, and system identification techniques. The main characteristics of this model are provided later on, but the readers can find many more details in [21, 22] and in the references therein. This model provides load outputs for the shear force as well as the torsional and bending moments at seven different load stations: six per wing and one for the horizontal tail. The overall structure of the model follows a modal approach, where the nonlinear rigid-body motion is complemented by a series of flexible modes (second-order linear structure, but the corresponding aerodynamic terms can principally include nonlinearities).

The equations of the rigid-body dynamics are expressed in the body axis system in Eq. (1). The rotational kinematic equations are expressed based on Euler angles in Eq. (2), whereas the translational kinematic equations are expressed in a geodetic frame (flat and fixed Earth assumption) in Eq. (3), see [23] for more details. The relationship between the components of the inertial, wind and aerodynamic velocity vectors is given by Eq. (4), whereas the definition of the corresponding flow and path angles will be given later when needed.

Table 1 DLR's Discus-2c Geometry and Mass Characteristics

Parameter	Value
Chord, m	0.685
Span, m	18
Wing area, m^2	11.39
m (with pilot 1 or 2), kg	451 or 422
I_{xx}, $kg.m^2$	3190
I_{yy}, $kg.m^2$	870
I_{zz}, $kg.m^2$	3900
$I_{xy} = I_{yz} = I_{xz}$	0

$$
\begin{aligned}
m\left(\dot{u}_K + qw_K - rv_K\right) + mg\sin\Theta &= \mathrm{X} \\
m\left(\dot{v}_K + ru_K - pw_K\right) - mg\cos\Theta\sin\Phi &= Y \\
m\left(\dot{w}_K + pv_K - qu_K\right) - mg\cos\Theta\cos\Phi &= Z \\
I_{xx}\dot{p} - I_{xy}\left(\dot{q} - pr\right) - I_{xz}\left(\dot{r} + pq\right) - I_{yz}\left(q^2 - r^2\right) + \left(I_{zz} - I_{yy}\right)qr &= L \\
I_{yy}\dot{q} - I_{xy}\left(\dot{p} + qr\right) - I_{yz}\left(\dot{r} - pq\right) + I_{xz}\left(p^2 - r^2\right) + \left(I_{xx} - I_{zz}\right)pr &= M \\
I_{zz}\dot{r} - I_{xz}\left(\dot{p} - qr\right) - I_{yz}\left(\dot{q} + pr\right) - I_{xy}\left(p^2 - q^2\right) + \left(I_{yy} - I_{xx}\right)pq &= N
\end{aligned}
\tag{1}
$$

$$
\begin{aligned}
\dot{\Phi} &= p + q\left(\sin\Phi\tan\Theta\right) + r\left(\cos\Phi\tan\Theta\right) \\
\dot{\Theta} &= q\cos\Phi - r\sin\Phi \\
\dot{\Psi} &= q\left(\sin\Phi\sec\Theta\right) + r\left(\cos\Phi\sec\Theta\right)
\end{aligned}
\tag{2}
$$

$$
\begin{aligned}
\dot{x} &= u_K\left(\cos\Theta\cos\Psi\right) + v_K\left(\sin\Phi\sin\Theta\cos\Psi - \cos\Phi\sin\Psi\right) + w_K\left(\cos\Phi\sin\Theta\cos\Psi + \sin\Phi\sin\Psi\right) \\
\dot{y} &= u_K\left(\cos\Theta\sin\Psi\right) + v_K\left(\sin\Phi\sin\Theta\sin\Psi + \cos\Phi\cos\Psi\right) + w_K\left(\cos\Phi\sin\Theta\sin\Psi - \sin\Phi\cos\Psi\right) \\
\dot{z} &= -u_K\sin\Theta + v_K\left(\sin\Phi\cos\Theta\right) + w_K\left(\cos\Phi\cos\Theta\right)
\end{aligned}
\tag{3}
$$

$$
\begin{aligned}
u &= u_K - u_W \\
v &= v_K - v_W \\
w &= w_K - w_W
\end{aligned}
\tag{4}
$$

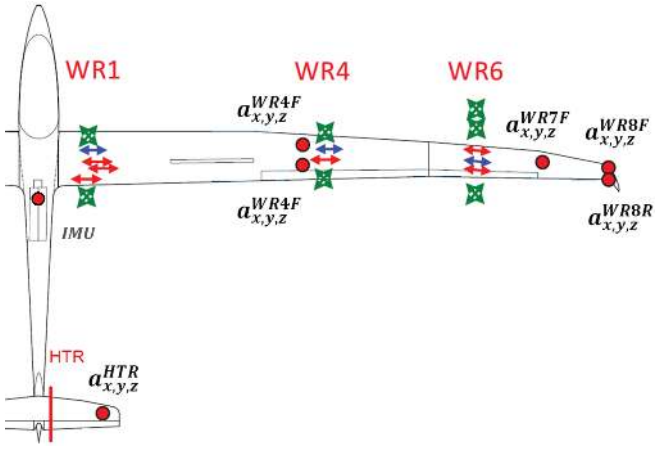

Fig. 2 DLR's Discus-2c Load Stations and Distribution of Measurement Sensors (red circles: accelerometers)

The total elastic displacement of a structure can be expressed in terms of modal expansion using n free-vibration modes as in Eq. (5), whereas the n generalized coordinates associated with the respective n free-vibration modes are governed by the n equations given by Eq. (6).

$$d_E(x, y, z, t) = \sum_{i=1}^{n} \phi_i(x, y, z)\, \eta_i(t) \tag{5}$$

$$\ddot{\eta}_i + 2\zeta_i \omega_i \dot{\eta}_i + \omega_i^2 \eta_i = \frac{Q_i}{m_i}, i = 1, 2, \cdots, n \tag{6}$$

By using the mean axis system (one at which the relative translational and angular momenta about the center of mass resulting from elastic deformation of a structure undergoing free vibration diminish), the equations of motion of the rigid body and the structural vibrations become uncoupled (except for the external forces and moments and the generalized forces), see [24]. Hence, an aeroelastic model is constituted of Eqs. (1-3 , 6). These equations are 12+n in number, have 12+2 n states, and are nonlinear coupled differential equations of first and second order.

To complete the aeroelastic model, expressions for the external forces and moments (aerodynamic model) and the generalized forces are needed. The aerodynamic model used in this work is expressed as partial derivatives of the motion variables, control surface inputs, and the flexible degrees of freedom of the aircraft. For the example aircraft used for the simulation in this work, these derivatives had been obtained by system identification from flight tests (see [21, 22] for further details).

C. The Discus-2c Control Design Model

The model described in the previous section is trimmed for a steady flight and linearized at this trimmed flight condition (see [25] for the comparison between this linear model and the nonlinear one of the example airplane considered in this work). The resulting linear model is then expressed as a continuous linear state-space. During or after the linearization, some states (i.e. modes) can be removed in order to obtain a smaller simplified model that is better suited for control synthesis purposes.

In this work, the model used for the control synthesis consists only of the short-period mode, the first and second wing bending modes (see Table. 2), the first-order transfer functions of the elevator and symmetric aileron actuator dynamics, in addition to the dynamics of any included filters or weighting functions as will be shown later.

Table 2 DLR's Discus-2c Modal Characteristics (in vacuum)

	Mode	
Parameter	1	2
Description	1^{st} wing vertical bending	2^{nd} wing vertical bending
Generalized mass, kg.cm^2	20	10.35
Frequency, rad/s	16.02	48.59
Damping ratio	0	0

IV. Proposed Control Design Methodology

The primary objective of the gust load alleviation controller is to minimize the impact of turbulence and gusts on the dynamic loads experienced by the structure. A secondary objective is that the load factor at the pilot location (and possibly at other locations) shall be reduced. In other words, the impact of the disturbance on the loads and load factor should be minimized: this is a disturbance rejection problem. In the following, we propose minimizing this impact in the sense of H_∞ norm.

A. The H_∞ Optimal Control

As already mentioned, the problem of ride qualities enhancement and structural loads alleviation of an aircraft when encountering turbulence or gusts is by nature a disturbance rejection problem, which can be well expressed as an H_∞ control design problem. In this type of problems, a controller, that stabilizes the closed-loop transfer function

from the so-called exogenous input to the regulated output while minimizing its gain, is synthesized. For multi-input multi-output (MIMO) systems, the transfer functions become transfer matrices. In this case, a relevant measure of the gain is a matrix norm. Two of the most widely-used norms are the H_2 and H_∞ norms. As the gust input is neither fixed nor has a fixed power spectrum, the H_∞ norm (peak gain of the closed-loop transfer function across all frequencies and all input directions) is better suited here. The following subsection gives a very short introduction to the H_∞ optimal control problem, to allow easier understanding of the following sections.

The concept of H_∞ control has been introduced in the late 1970's and early 1980's. The standard H_∞ control problem is illustrated in Fig. 3, where P is the generalized plant (the plant plus all weighting functions) and K is the controller to be synthesized. $\boldsymbol{w}$, $\boldsymbol{z}$, $\boldsymbol{u}$ and $\boldsymbol{y}$ (in **bold** to be differentiated from the symbols used in the aeroelastic model) are the exogenous input, regulated output, control input, and measured output vectors, respectively. The generalized plant P can be expressed in state-space form as in Eqs. (7) , where $\boldsymbol{x}$ (in **bold**) is the system state vector. The matrices A, B_1, B_2, C_1, C_2, D_{11}, D_{12}, D_{21} and D_{22} are of appropriate dimensions. This figure basically consists of a lower linear fractional transformation (LFT), with the generalized plant's measured outputs being fed back to its control inputs through the controller K. The objective of the H_∞ control design is to find the controller K that stabilizes P and ensures that the infinity norm of the closed-loop transfer matrix from the exogenous input to the regulated output, $\|T_{\boldsymbol{zw}}\|_\infty$, is less than a positive H_∞ performance value γ (i.e., $\|T_{\boldsymbol{zw}}\|_\infty<\gamma$). The term H_∞ itself is derived from the corresponding Hardy space (see [26, 27]), and can also be seen as a particular case of the L_2-induced norm in case of linear dynamic systems.

$$\begin{aligned} \dot{\boldsymbol{x}}(t) &= A\boldsymbol{x}(t) + B_1\boldsymbol{w}(t) + B_2\boldsymbol{u}(t) \\ \boldsymbol{z}(t) &= C_1\boldsymbol{x}(t) + D_{11}\boldsymbol{w}(t) + D_{12}\boldsymbol{u}(t) \\ \boldsymbol{y}(t) &= C_2\boldsymbol{x}(t) + D_{21}\boldsymbol{w}(t) + D_{22}\boldsymbol{u}(t) \end{aligned} \tag{7}$$

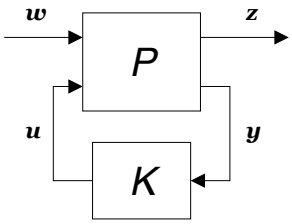

Fig. 3 Standard Form for Control Synthesis

Controllers which are synthesized with H_∞ techniques are often considered as "robust controllers" due to the interpretation of the H_∞-norm as a robustness margin (interpretation resulting from the "small-gain theorem" in the case of linear time-invariant (LTI) systems, see [26–28]). The basic idea of this theorem for the interconnection of Fig. 3 can be expressed as follows: Let $\gamma = \|T_{\boldsymbol{zw}} = F_l(P,K)\|_\infty$, where F_l is the lower LFT. Then the output $\boldsymbol{z}$ can be fed back to the input $\boldsymbol{w}$ through any system Δ such that $\|\Delta\|_\infty < \gamma$, without destabilizing the closed-loop $F_u(F_l(P,K),\Delta)$, where F_u is the upper LFT. As a consequence, if the input $\boldsymbol{w}$ and the output $\boldsymbol{z}$ are chosen such that closing the loop from $\boldsymbol{z}$ to $\boldsymbol{w}$ can be interpreted physically as taking a meaningful set of uncertainties into account, then minimizing the H_∞-norm from $\boldsymbol{w}$ to $\boldsymbol{z}$ leads to increasing the robustness of the closed-loop.

It is however crucial to understand that the H_∞ techniques can also be used as a mean to "shape" some particular transfer function for the closed loop. In such cases, feeding the regulated output $\boldsymbol{z}$ back to the exogenous input $\boldsymbol{w}$ through an uncertainty block Δ often does not correspond to anything meaningful for the considered application. In other words, if neither unmodeled dynamics nor parametric uncertainties are expected between $\boldsymbol{z}$ and $\boldsymbol{w}$, then the interpretation of the H_∞ norm $\|T_{\boldsymbol{zw}} = F_l(P,K)\|_\infty$ as a robustness measure is not useful. H_∞ techniques can be used to increase robustness, but the sole fact that H_∞ techniques have been used does necessarily mean that the obtained closed-loop is robust (i.e., the achieved performance and the performance channel definition must be analyzed to be able to conclude on robustness). In this paper, the H_∞ techniques are only used to specify the desired load alleviation behavior (i.e. to shape the gust/turbulence rejection), with and without preview of the disturbance. The solutions obtained were found to be quite robust, but exhaustive robustness analysis as well as adding specific criterion to explicitly ensure robustness during the control synthesis are let for further work.

Traditionally, two main approaches [29, 30] have been widely used to synthesize H_∞ controllers. Both are algorithmically quite efficient, even though their $O(N^4)$ complexity (N being the number of states of the control

design plant) tend to strongly limit the size of the problems they can be applied to. These methods have the following disadvantages:

1) They provide no way to impose a certain required structure of the controller
2) They require the expression of all design requirements in terms of a single MIMO transfer function
3) The order of the synthesized controller is the same as that of the weighted plant P. This often causes issues with their practical implementation, and the controller must be simplified or reduced a posteriori, which is often far from being trivial.

As a response to the need to tackle these disadvantages, various other methods were investigated; for instance, the approach in [31]. This approach has two advantages over the classical full-order synthesis algorithms:

1) It allows the synthesis of controllers for models with multi performance channels
2) It can synthesize controllers with all kinds of structures and orders, as long as they remain linear

This also means that if the designer correctly specified the structure of the desired controller, then the implementation of the obtained controller in a real-time embedded system should be straightforward (i.e., no controller reduction is required). However, this approach has the disadvantage of solving a non-convex problem based on local optimization techniques and multiple random restarts (see [32]); which in turn, increases the computation time and there is *a priori* no guarantee of reaching the global optimum. In practice, the advantages of this method often make up for its disadvantages.

B. Preview Control

By measuring the disturbance ahead of the plant with enough lead time, new information and degrees of freedom become available for the controller; hence, a performance enhancement can be achieved. This type of control strategies has been used for various systems, see for instance [33–37] and the references therein, under the name "preview control".

In the present paper, it is assumed (with no further discussion) that a sensor system is able to measure the vertical wind ahead of the aircraft; therefore, the vertical wind over a small time horizon in the future is known. The interested reader is referred to [16, 17, 38] and the references therein for further information on the sensor technologies that could provide this capability. This paper focuses rather on the question of the optimal exploitation of the previewed disturbance, and does not tackle the question of how to obtain this information in practice. This preview control approach proposed here can be seen as a direct extension of [17–20] in which the controllers were sub-optimally manually tuned based on the designer's understanding of flight mechanics and aeroelasticity.

Note also that in practice for the considered application, the sensor is measuring the wind at the current time, but at a location that the aircraft has not reached yet. Even if (in the considered configuration) the measured wind is not expected to change significantly during the time the aircraft needs to reach the measurement location, it could theoretically change; and the correct physical interpretation is that it is a remote measurement, and not a glimpse into the future. Based on the remote wind information gathered ahead of the aircraft at the present time and in the past and based on the aircraft motion, a "best guess" on the future encountered gust/turbulence is made and used to anticipate and alleviate the resulting structural loads.

Preview control problems can typically be represented by the block diagram of Fig. 4. Note that the control problem of Fig. 4 is causal because instead of considering that the controller knows the disturbance in advance (which would not lead to a causal system), we consider (without loss of generality) that the disturbance measured at the current time will affect the system P after a time delay $\boldsymbol{h}$. The system P can be expressed in state-space form as in Eq. (8), where $\boldsymbol{w}$ is as before the exogenous input (chosen in this work to be the previewed disturbance input, $\boldsymbol{d_p}$).

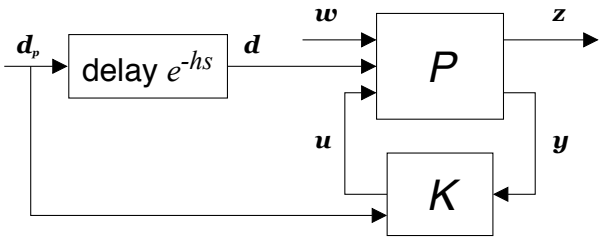

Fig. 4 Feedforward-Feedback Preview Control Architecture

$$\begin{aligned} \dot{\boldsymbol{x}}(t) &= \tilde{A}\boldsymbol{x}(t) + \tilde{B}_1\boldsymbol{d}(t) + \tilde{B}_2\boldsymbol{u}(t) \\ z(t) &= \tilde{C}_1\boldsymbol{x}(t) + \tilde{D}_{11}\boldsymbol{d}(t) + \tilde{D}_{12}\boldsymbol{u}(t) \\ \boldsymbol{y}(t) &= \tilde{C}_2\boldsymbol{x}(t) + \tilde{D}_{21}\boldsymbol{d}(t) + \tilde{D}_{22}\boldsymbol{u}(t) \end{aligned} \tag{8}$$

In the literature, two different main approaches to account for the delay term are followed. The first is in the continuous-time domain and based on the work of [34, 35], whereas the second is in the discrete-time domain and based on the work of [37]. In the course of this work, a discrete-time formulation, strongly inspired by the one used in [37], is used. In the discrete-time approach of [37], the problem had been formulated as a full information state-feedback control problem and solved using state augmentation technique. Since in our case, the model dynamics are of flexible aircraft (i.e. include flexible degrees of freedom that cannot be measured), an output-feedback formulation is made and used in the following.

The system (Eqs. (8)) is converted to the discrete-time domain as in Eqs. (9). The previewed information is simply modeled in the discrete-time formulation as a chain of unit delays that augments the open-loop state-space representation of the plant P by $\boldsymbol{h}$ states, where $\boldsymbol{h}$ is now a nonnegative constant called the preview length (= the preview time divided by the sampling time). The physical interpretation of this chain of unit delays can be seen in Fig. 5, where the values of $\boldsymbol{d}(k)$, $\boldsymbol{d}(k+1)$, $\cdots$, $\boldsymbol{d}(k+\boldsymbol{h})$ are available for control.

$$\begin{aligned} \dot{\boldsymbol{x}}(k+1) &= A\boldsymbol{x}(k) + B_1\boldsymbol{d}(k) + B_2\boldsymbol{u}(k) \\ z(k) &= C_1\boldsymbol{x}(k) + D_{11}\boldsymbol{d}(k) + D_{12}\boldsymbol{u}(k) \\ \boldsymbol{y}(k) &= C_2\boldsymbol{x}(k) + D_{21}\boldsymbol{d}(k) + D_{22}\boldsymbol{u}(k) \end{aligned} \tag{9}$$

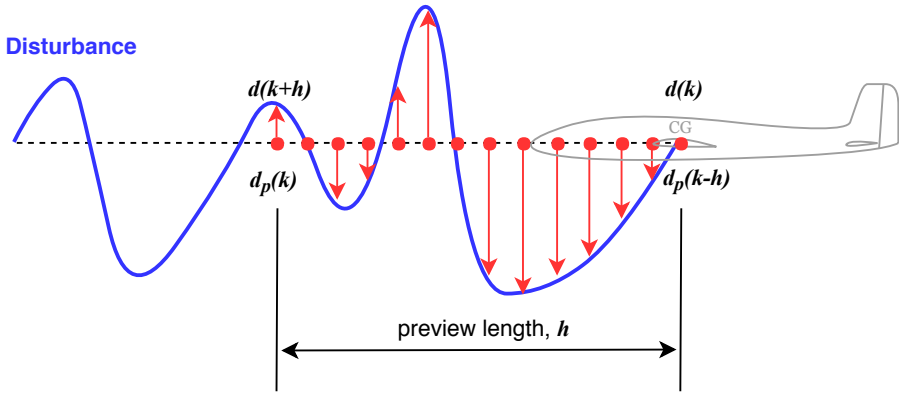

Fig. 5 The Previewed Disturbance Input ahead of the Aircraft and its Sampling

The following state-space representation of this chain of unit delays has been chosen. By defining the state vector $x_d = [\boldsymbol{d}(k)\,\boldsymbol{d}(k+1)\cdots\boldsymbol{d}(k+\boldsymbol{h})]^T = \left[\boldsymbol{d_p}(k-\boldsymbol{h})\,\boldsymbol{d_p}(k-\boldsymbol{h}+1)\cdots\boldsymbol{d_p}(k)\right]^T$, then x_d is related to d_p by the state-space of Eq. (10), where the corresponding matrices are defined in Eq. (11). In this output-feedback formulation, the current value of $\boldsymbol{d_p}$ is also used for control, which is different from the state-feedback formulation of [37].

$$\begin{aligned} x_d(k+1) &= A_d x_d(k) + B_d\boldsymbol{d_p}(k) \\ y_d(k) &= C_d x_d(k) + D_d\boldsymbol{d_p}(k) \end{aligned} \tag{10}$$

$$A_d = \left[\begin{array}{c|c} \boldsymbol{0}_{h-1\times 1} & \boldsymbol{I}_{h-1\times h-1} \\ \hline 0 & \boldsymbol{0}_{1\times h-1} \end{array}\right], B_d = \left[\begin{array}{c} \boldsymbol{0}_{h-1\times 1} \\ \hline 1 \end{array}\right], C_d = \left[\begin{array}{c} \boldsymbol{I}_{h\times h} \\ \hline \boldsymbol{0}_{1\times h} \end{array}\right], D_d = \left[\begin{array}{c} \boldsymbol{0}_{h\times 1} \\ \hline 1 \end{array}\right] \tag{11}$$

In case of zero preview (i.e., $\boldsymbol{h} = 0$), Eq. (10) simply reduces to the output equation Eq. (12), with no state equation.

$$y_d(k) = \boldsymbol{d_p}(k) \tag{12}$$

The model of Eq. (9) is named $G(z)$ in the following. Its augmentation with the aforementioned chain of unit delays is made as shown in Fig. 6. In this diagram, the previewed disturbance input $\boldsymbol{d_p}$ and the performance channel input $\boldsymbol{w}$

are defined as two separate inputs, in order to keep this representation as general as possible. In the herein considered pure disturbance rejection problem, $\boldsymbol{d_p}$ will also be the input of the performance channel (i.e., the connection between $\boldsymbol{w}$ and $G(z)$ would then be removed and the performance channel is the transfer function from $\boldsymbol{d_p}$ to $\boldsymbol{z}$). In another context or in a multi-channel problem, $\boldsymbol{w}$ could be another interesting physical input (e.g., another type of disturbance which can neither be measured nor previewed, but also to be rejected by the closed loop), or various signals could be previewed with different preview horizon for each. As a consequence, Fig. 6 should be understood as a generic sketch of the different ways the original plant can be augmented for including preview signals, rather than the only augmentation scheme considered here.

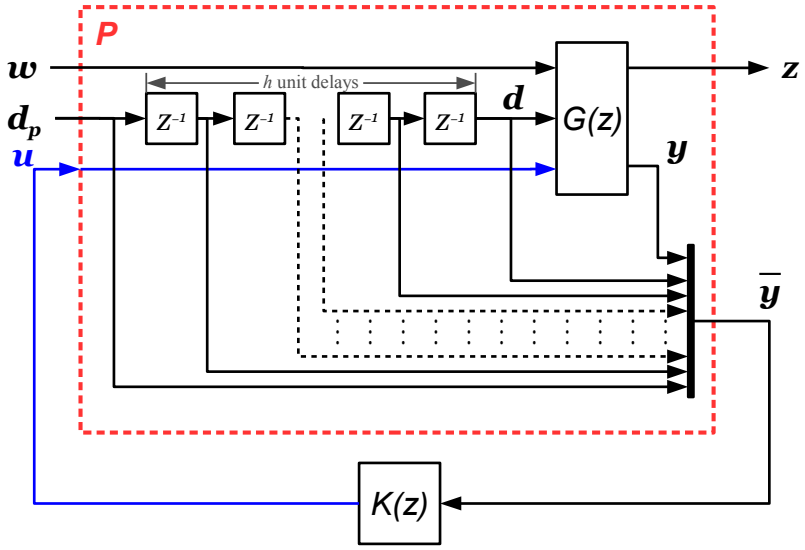

Fig. 6 Augmentation of the Discrete-Time H_∞ Control Design Plant with the Previewed Disturbance

The equations corresponding to the augmented system of Fig. 6 (with $\boldsymbol{w} = \boldsymbol{d_p}$) can be written using the augmented state vector $\xi((k)) = \left[\left[\boldsymbol{x}^{\boldsymbol{T}}(k)\, x_d^T(k)\right]^T\right.$. By combining Eq. (9) and Eq. (10), the final augmented system can be expressed as in Eq. (13), where the corresponding matrices are defined by Eq. (14). The system (Eqs. (13)) is in the standard form of the H_∞ optimal control given by Eqs. (7); hence, the characterization of solvability relies exclusively on that of the H_∞ optimal control theory. This allows for tackling the disadvantages of the continuous-time approach; but on the other hand, this discrete-time approach has the following disadvantages:

1) The plant should be discretized (with the known accompanying problems and precautions of discretization)
2) The system order (and hence the controller order if the full-order method is used) becomes a function in the preview length

$$\begin{aligned} \dot{\boldsymbol{\xi}}(k+1) &= \overline{A}\xi(k) + \overline{B}_1\boldsymbol{d_p}(k) + \overline{B}_2\boldsymbol{u}(k) \\ \boldsymbol{z}(k) &= \overline{C}_1\xi(k) + \overline{D}_{11}\boldsymbol{d_p}(k) + \overline{D}_{12}\boldsymbol{u}(k) \\ \overline{\boldsymbol{y}}(k) &= \overline{C}_2\xi(k) + \overline{D}_{21}\boldsymbol{d_p}(k) + \overline{D}_{22}\boldsymbol{u}(k) \end{aligned} \tag{13}$$

$$\overline{A} = \left[\begin{array}{c|cc} A & B_1 & \mathbf{0}_{n_x\times h-1} \\ \hline \mathbf{0}_{h\times n_x} & \multicolumn{2}{c}{A_d} \end{array}\right], \overline{B}_1 = \left[\begin{array}{c} \mathbf{0}_{n_x\times 1} \\ \hline B_d \end{array}\right], \overline{B}_2 = \left[\begin{array}{c} B_2 \\ \hline \mathbf{0}_{h\times n_u} \end{array}\right]$$

$$\overline{C}_1 = \left[\begin{array}{c|cc} C_1 & D_{11} & \mathbf{0}_{n_z\times h-1} \end{array}\right], \overline{D}_{11} = \left[\begin{array}{c} \mathbf{0}_{n_z\times 1} \end{array}\right], \overline{D}_{12} = D_{12} \tag{14}$$

$$\overline{C}_2 = \left[\begin{array}{c|cc} C_2 & D_{21} & \mathbf{0}_{n_y\times h-1} \\ \hline \mathbf{0}_{h+1\times n_x} & \multicolumn{2}{c}{C_d} \end{array}\right], \overline{D}_{21} = \left[\begin{array}{c} \mathbf{0}_{n_y\times 1} \\ \hline D_d \end{array}\right], \overline{D}_{22} = \left[\begin{array}{c} D_{22} \\ \hline \mathbf{0}_{h+1\times n_u} \end{array}\right]$$

V. Results

In this section, first the H_∞ performance channel(s) will be normalized; followed by including additional weights to express the desired performance, compared to the baseline performance (chosen here to be the open-loop). Second, the results obtained for the Discus-2c sailplane model will be shown.

A. Normalization and Weighting Functions

The state-space model resulting from the linearization of the nonlinear aeroelastic model of the aircraft dynamics cannot be directly used for the H_∞ optimal control synthesis, as the regulated output channels are in general of different weights and dimensions. A normalization process should be done first. In this work, a discrete-gust design criteria of the Airworthiness Standards: Transport Category Airplanes (14 CFR 25.341 / CS-25.341) is followed for such a normalization. According to this approach, a gust of 1-cos shape with different sufficient number of gust gradient distances in the range 30 feet to 350 feet (9 m to 107 m) must be investigated to find the critical response for each load quantity. Since this gust design criteria is for transport airplanes, but the model aircraft used for the simulation is a sailplane, the gust gradient and the maximum design gust velocity of the criteria had been scaled down by the ratio of the trim speed of DLR's Discus-2c (160 km/hr at altitude of 1000 m) to that of a transport airplane (assumed Mach 0.5). After that, each regulated output channel is divided by its corresponding maximum absolute load resulting from these gust loads. The advantage of this approach of normalization is that it relies on physical representative quantities; hence, it results in a normalized state-space model of the aircraft dynamics that is independent of the form of the state-space representation itself. In Fig. 7, the regulated output channels are shown for different gust gradient distances. The resulting maximum and minimum structural loads (from which the corresponding maximum absolute values are selected for the normalization) are shown in Fig. 8. The same procedure is applied for the structural loads and the load factors at other different stations (but not shown in the graph).

After that, the weighting functions are to be selected, which depend on the selected regulated output channels. The model used in this work has 7 regulated output channels: 1) one for the load factor at pilot location (n_z^{pilot}, non-dimensional), 2) one for the shear force at wing station WR1 (SR1, in Newton), 3) one for the torsional moment at wing station WR1 (TR1, in Newton-meter), 4) one for the bending moment at wing station WR1 (BR1, in Newton-meter), 5) one for the load factor at horizontal tail station HTR (n_z^{HTR}, non-dimensional), 6) one for the elevator control action, and 7) one for the symmetric aileron control action. The weighting functions of the elevator and the symmetric aileron control actions are selected to penalize the high-frequency dynamics (i.e., lead compensator or realizable high-pass filter), considering the respective dynamics of each control surface actuator. All other weighting functions are selected to be static gains. Afterwards, all the gains of the weighting functions are adjusted so that the feedback-only case has an H_∞ norm that is approximately 15 percent less than that of the open-loop system.

B. Full-Order and Fixed-Structure H_∞ Optimal Control with Preview

In this subsection, the simulation results will be shown for both synthesis methods: full-order and Fixed-Structure H_∞ optimal control with preview. In Fig. 9, it can be seen that the H_∞ performance value γ decreases monotonically with increasing the preview length (or the preview time) until reaching a lowest value. After reaching this lowest value, no more performance enhancement could be obtained even with increasing the preview length.

From Fig. 9, it can also be seen that almost the same performance can be obtained with the Fixed-Structure H_∞ optimal control method, but with a significantly lower controller order (controller order = 2 and 6 are shown) than that of the Full-Order one (controller order = 10 [aircraft, actuators and weighting functions states] + $\boldsymbol{h}$+1 [preview]).

In Fig. 10, this enhancement in the H_∞ performance value can be seen as a reduction in the maximum absolute values of the time response of the different regulated outputs when encountering the gust.

The rigid-body states (w_K and q), the flexible degrees of freedom (η_1, η_3, $\dot{\eta}_1$, and $\dot{\eta}_3$), the kinematic angle of attack $\alpha_K = \arcsin \frac{w_K}{V_\infty}$, the angle of attack $\alpha = \arcsin \frac{w}{V_\infty} = \arcsin \frac{w_K - w_W}{V_\infty}$ and the regulated outputs are shown in the time domain in Fig. 11. In this figure, it can be seen that the controller strategy is to use the previewed gust to actuate, in advance, the elevator and symmetric aileron, to enhance the performance. More specifically, the controller actuates the two control surfaces to: 1) damp the structural motion together with affecting the rigid-body motion, which results in alleviating the structural loads, and 2) to pitch and heave the aircraft together with affecting the structural motion, which results in decreasing the load factors.

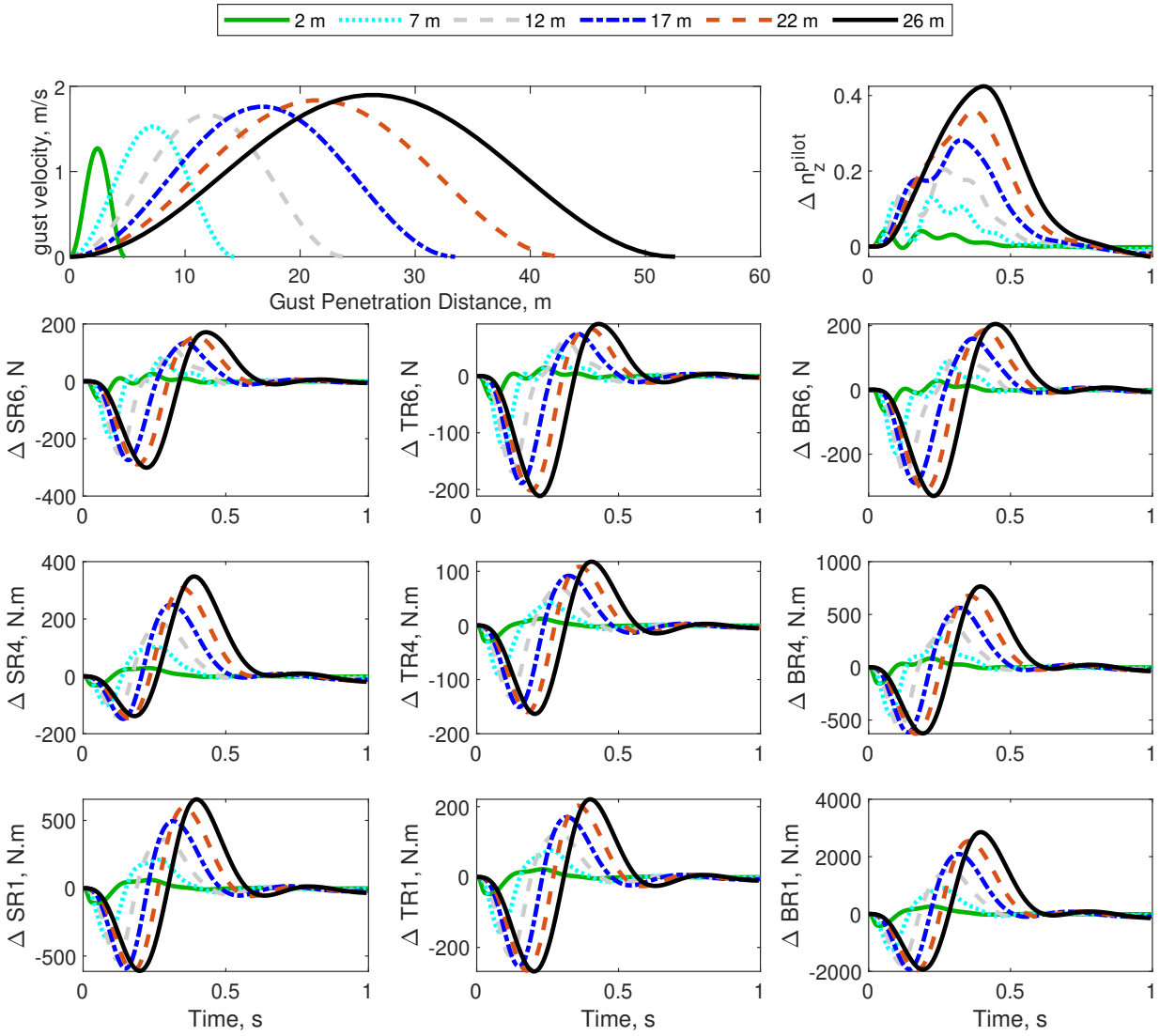

Fig. 7 Regulated Output Channels for 1-cos Vertical Gust at Different Gust Gradient Distances

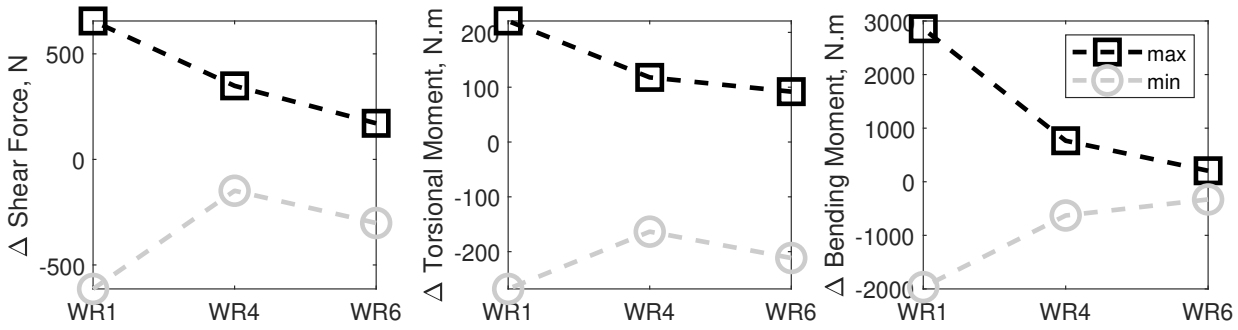

Fig. 8 Maximum and Minimum (Structural) Loads used for the Normalization

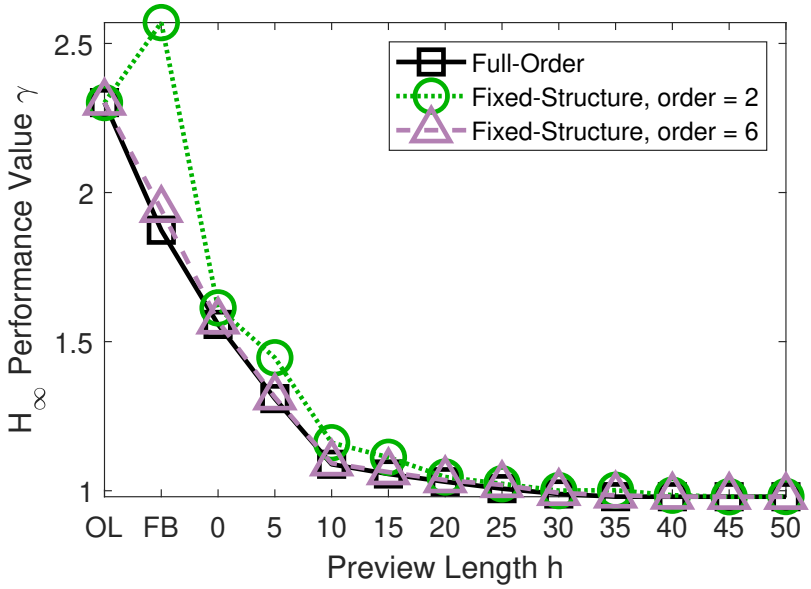

Fig. 9 H_∞ Performance Value as Function in Preview Time for Full-Order and Fixed-Structure (with different controller orders) Synthesis Methods (OL: Open-Loop, FB: Feedback-Only)

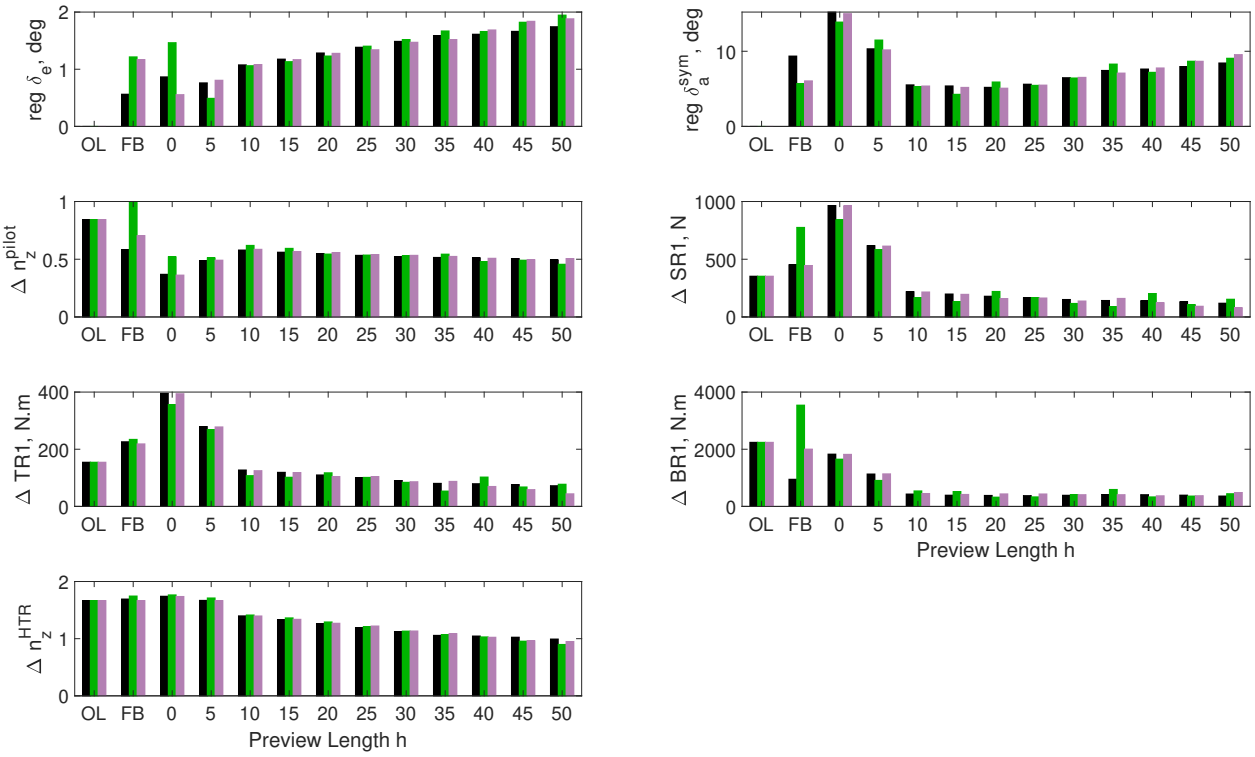

Fig. 10 Maximum Absolute Values of the Regulated Outputs as Function in Preview Time for Full-Order and Fixed-Structure (with different controller orders) Synthesis Methods (Black: Full-Order, Green: Fixed-Structure order 2, Violet: Fixed-Structure order 6)

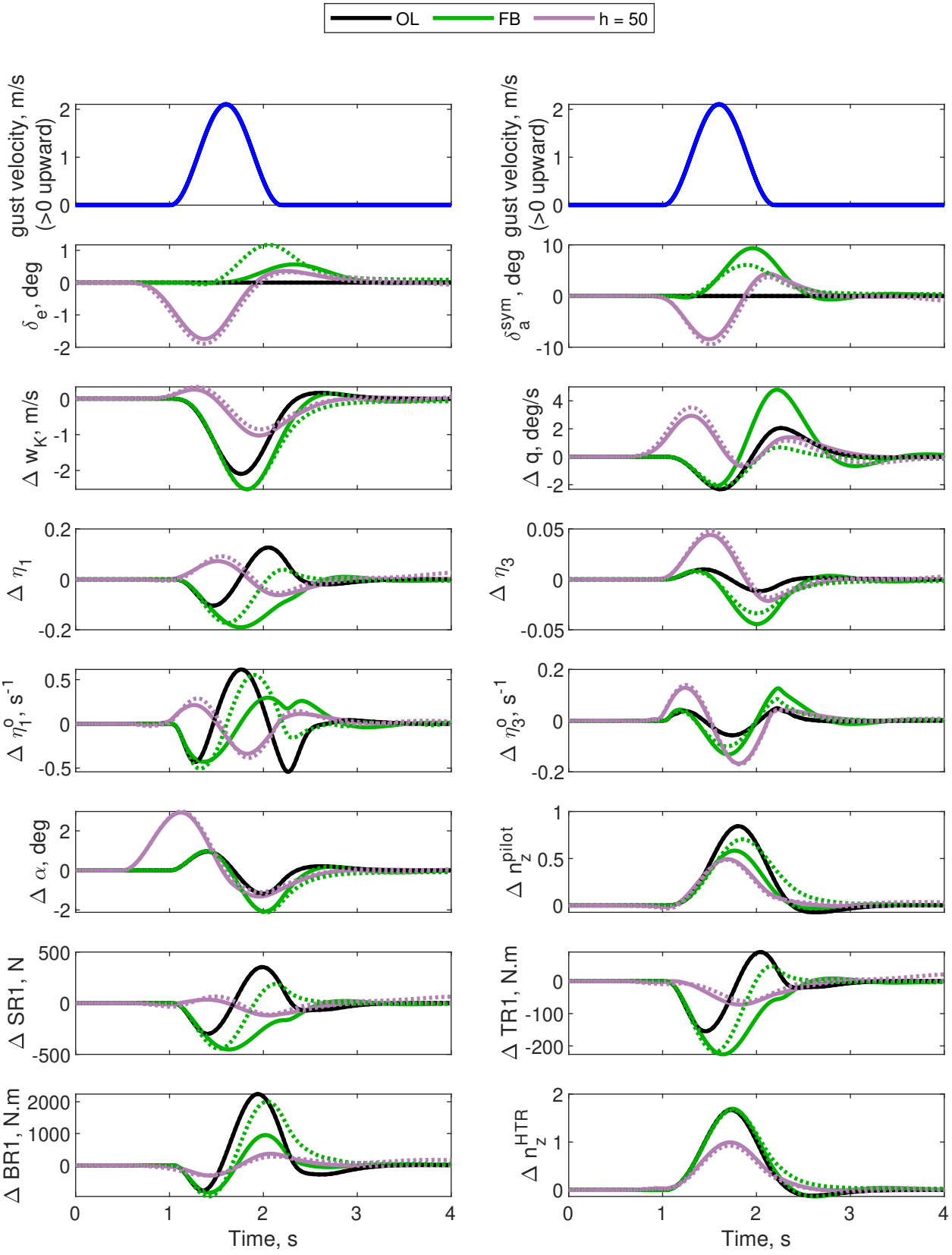

Fig. 11 Aircraft States and Regulated Outputs for Full-Order (solid lines –) and Fixed-Structure (dotted lines ···) Synthesis Methods in case of Open-Loop, Feedback-Only, and with Preview Length = 50

VI. Conclusion

In this work, a new approach for control synthesis has been suggested to enhance the performance of the GLAS of flexible aircraft. The approach relies on using new sensor technology of airborne Doppler LIDAR for determining in advance the gust disturbances that the aircraft will encounter. This future information of gust disturbances is then used in the control action, as what is known by preview control. The problem has been formulated in the course of this work to be in the standard form of the H_∞ optimal control synthesis. Two methods for synthesizing the H_∞ optimal controller had been applied: a full-order one and a fixed-structure one. The advantages and disadvantages of each of the two synthesis methods had been discussed and shown through simulation on a flexible aircraft model. The simulation results have shown that the suggested approach has effectively enhanced the performance of the GLAS; and that by comparing the fixed-structure synthesis method to the full-order one, almost the same performance can be achieved, but with the advantage of much lower controller order.

Acknowledgments

The first author would like to thank Dipl.-Ing. Per ohme, Dr.-Ing. Holger Duda, and Dipl.-Ing. Wulf Mönnich from DLR's Institute of Flight Systems for their appreciated support and helpful discussions. The first author would like also to thank the German Academic Exchange Service (Deutscher Akademischer Austauschdienst, DAAD) for funding his research stay at DLR. The work of the second author has been funded within the frame of the Joint Technology Initiative JTI Clean Sky 2, AIRFRAME Integrated Technology Demonstrator platform "AIRFRAME ITD" (contract N° CSJU-CS2-GAM-AIR-2014-15-01 Annex 1, Issue B04, October 2nd, 2015) being part of the Horizon 2020 research and Innovation framework programme of the European Commission. The methodology presented in this paper will be applied to large transport airplanes and business jets within the CleanSky2 NACOR project funded, among many others, through the aforementioned contract.

References

[1] ISO 1151-1:1988(E), "Flight dynamics – Concepts, quantities and symbols – Part 1: Aircraft motion relative to the air," Standard, International Organization for Standardization, Geneva, CH, Apr. 1988.

[2] ISO 1151-2:1985(E), "Flight dynamics – Concepts, quantities and symbols – Part 2: Motions of the aircraft and the atmosphere relative to the Earth," Standard, International Organization for Standardization, Geneva, CH, Sep. 1985.

[3] Hargrove, W. J., "The C-5A active lift distribution control system," Tech. Rep. 76N31148, NASA, August 1976.

[4] Regan, C. D., and Jutte, C. V., "Survey of Applications of Active Control Technology for Gust Alleviation and New Challenges for Lighter-weight Aircraft," Tech. Rep. NASA/TM-2012-216008, DFRC-E-DAA-TN4736, NASA, April 2012.

[5] Hoffmann, G., "Stabilisierung, Böenkompensation und Schwingungsdämpfung am elastischen beweglichen Flugzeugmodell im Windkanal," Tech. Rep. DLR-FB 76-44, DFVLR (now part of DLR), 1976.

[6] Krag, B., "The wind tunnel behaviour of a scaled model with a gust alleviation system in a deterministic gust field," *Transactions of the Institute of Measurement and Control*, Vol. 1, No. 3, 1979, pp. 141–153. doi:https://doi.org/10.1177/014233127900100303.

[7] Böhret, H., Krag, B., and Skudridakis, J., "OLGA – An Open-Loop Gust Alleviation System," *AGARD CP 384 Meeting*, Toronto, Canada, 1985.

[8] König, R., and Hahn, K.-U., "Load Alleviation and Ride Smoothing Investigations Using ATTAS," *17th Congress of the International Council of the Aeronautical Sciences*, Stockholm, Sweden, 1990.

[9] Hahn, K.-U., and König, R., "ATTAS Flight Test and Simulation Results of the Advanced Gust Management System LARS," *AIAA Atmospheric Flight Mechanics Conference*, Hilton Head, SC, USA, 1992.

[10] König, R., Hahn, K.-U., and Winter, J., "Advanced Gust Management Systems - Lessons Learned and Perspectives," *AGARD Flight Mechanics Panel Symposium on Active Control Technology: Applications and Lessons Learned*, Torino, Italy, 1994.

[11] Hecker, S., and Hahn, K.-U., "Gust Computation System," Tech. Rep. DLR-TR-3.1.1-11, AWIATOR, DLR, May 2003.

[12] Hahn, K.-U., and Hecker, S., "Gust Load Alleviation System," Tech. Rep. DLR-TR-3.1.1-12, AWIATOR, DLR, April 2004.

[13] Hecker, S., and Hahn, K.-U., "Proposal of gust load alleviation system using adaptive elements," Tech. Rep. DLR-TR-3.1.1-13, AWIATOR, DLR, 2005.

[14] Hecker, S., and Hahn, K.-U., "Proposal of gust load alleviation system using turbulence sensor and adaptive elements," Tech. Rep. DLR-TR-3.1.1-14, AWIATOR, DLR, July 2006.

[15] Schmitt, N. P., Rehm, W., Pistner, T., Zeller, P., Reithmeier, G., Stilkerich, S., Schertler, K., Diehl, H., and Zinner, H., "The AWIATOR Airborne LIDAR Turbulence Sensor," *2005 German Aerospace Congress (Deutscher Luftund Raumfahrtkongress / DLRK)*, DGLR, Friedrichshafen, Germany, 2005.

[16] Rabadan, G. J., Schmitt, N. P., Pistner, T., and Rehm, W., "Airborne Lidar for Automatic Feedforward Control of Turbulent In-Flight Phenomena," *Journal of Aircraft*, Vol. 47, No. 2, 2010, pp. 392–403. doi:https://doi.org/10.2514/1.44950.

[17] Fezans, N., Schwithal, J., and Fischenberg, D., "In-flight remote sensing and identification of gusts, turbulence, and wake vortices using a Doppler LIDAR," *CEAS Aeronautical Journal*, Vol. 8, No. 2, 2017. Doi:10.1007/s13272-017-0240-9.

[18] Fezans, N., "An Unusual Structure for a Feedforward Gust Load Alleviation Controller," *Proceedings of the 2017 CEAS EuroGNC Conference*, Warsaw, Poland, 2017.

[19] Fezans, N., and Joos, H.-D., "Combined Feedback and LIDAR-Based Feedforward Active Load Alleviation," *AIAA Atmospheric Flight Mechanics Conference*, AIAA, Denver, Colorado, 2017. doi:https://doi.org/10.2514/6.2017-3548.

[20] Fezans, N., Joos, H.-D., and Deiler, C., "Gust load alleviation for a long-range aircraft withand without anticipation," *accepted for publication in the CEAS Aeronautical Journal*, 2018.

[21] Viana, M. V. P., "Time-Domain System Identification of Rigid-Body Multipoint Loads Model," *AIAA Atmospheric Flight Mechanics Conference*, AIAA, Washington, DC, 2016. doi:https://doi.org/10.2514/6.2016-3706.

[22] Viana, M. V. P., "Multipoint Model for Flexible Aircraft Loads Monitoring in Real Time," Tech. rep., DLR, 2016.

[23] Etkin, B., and Lloyd, D. R., *Dynamics of Flight: Stability and Control*, 3rd ed., Wiley, New York, 1996.

[24] Schmidt, D., *Modern Flight Dynamics*, 1st ed., McGraw-Hill Education, New York, 2012.

[25] Khalil, A., "Flight Dynamics, Handling and Ride Qualities of a Flexible Aircraft," *2017 German Aerospace Congress (Deutscher Luftund Raumfahrtkongress / DLRK)*, DGLR, Munich, Germany, 2017.

[26] Zhou, K., Doyle, J. C., and Glover, K., *Robust and optimal control*, Prentice Hall, 1996.

[27] Ackerman, J., *Robust Control - Systems with Uncertain Physical Parameters*, Springer-Verlag, 1993. ISBN 3-540-19843-1 / 0-387-19843-1.

[28] Khalil, H. K., *Nonlinear Systems*, 3rd ed., Prentice-Hall, 2002. ISBN: 0-13-067389-7.

[29] Doyle, J. C., Glover, K., Khargonekar, P. P., and Francis, B. A., "State-Space Solutions to Standard H_2 and H_∞ Control Problems," *IEEE Transactions on Automatic Control*, Vol. 34, No. 8, 1989, pp. 831–847. doi:http://doi.org/10.1109/9.29425.

[30] Gahinet, P., and Apkarian, P., "A Linear Matrix Inequality Approach to H_∞ Control," *Robust and Nonlinear Control*, Vol. 4, No. 4, 1994, pp. 421–448. doi:https://doi.org/10.1002/rnc.4590040403.

[31] Apkarian, P., and Noll, D., "Nonsmooth H_∞ Synthesis," *IEEE Transactions on Automatic Control*, Vol. 51, No. 1, 2006, pp. 71–86. doi:http://doi.org/10.1109/TAC.2005.860290.

[32] Apkarian, P., and Noll, D., *Optimization-Based Control Design Techniques and Tools*, Springer London, London, 2013, pp. 1–12. doi:http://doi.org/10.1007/978-1-4471-5102-9_144-1.

[33] Birla, N., and Swarup, A., "Optimal preview control: A review," *Optimal Control Applications and Methods*, Vol. 36, No. 2, 2014, p. 241–268. doi:10.1002/oca.2106.

[34] Kojima, A., and Ishijima, S., "H_∞ Performance of Preview Control Systems," *Automatica*, Vol. 39, 2003, pp. 693–701. doi:http://doi.org/10.1016/S0005-1098(02)00286-8.

[35] Kojima, A., and Ishijima, S., "H_∞ Preview Tracking in Output Feedback Setting," *Robust and Nonlinear Control*, Vol. 14, No. 7, 2004, p. 627–641. doi:https://doi.org/10.1002/rnc.897.

[36] Zattoni, E., "H_2-Optimal Rejection with Preview: Geometric Constraints and Dynamic Feedforward Solutions via Spectral Factorization," *Kybernetika*, Vol. 44, No. 1, 2008, p. 3–16.

[37] Takaba, K., "A Tutorial on Preview Control Systems," *IEEE SICE 2003 Annual Conference*, IEEE, Fukui, Japan, 2003.

[38] Herbst, J., and Vrancken, P., "Design of a monolithic Michelson interferometer for fringe imaging in a near-field, UV, direct-detection Doppler wind lidar," *Applied Optics*, Vol. 55, No. 25, 2016, pp. 6910–6929.